Spectral Appearance Changes Induced by Light Exposure

BRADLEY W. KIMMEL, GLADIMIR V. G. BARANOSKI, T. F. CHEN, DANIEL YIM, and ERIK MIRANDA
University of Waterloo

The fading of materials due to light exposure over time is a major contributor to the overall aged appearance of man-made objects. Although much attention has been devoted to the modeling of aging and weathering phenomena over the last decade, comparatively little attention has been paid to fading effects. In this article, we present a theoretical framework for the physically based simulation of time-dependent spectral changes induced by absorbed radiation. This framework relies on the general volumetric radiative transfer theory, and it employs a physicochemical approach to account for variations in the absorptive properties of colorants. Employing this framework, a layered fading model that can be readily integrated into existing rendering systems is developed using the Kubelka-Munk theory. We evaluate its correctness through comparisons of measured and simulated fading results. Finally, we demonstrate the effectiveness of this model through renderings depicting typical fading scenarios.

Categories and Subject Descriptors: I.3.7 [**Computer Graphics**]: Three-Dimensional Graphics and Realism—*Color, shading, shadowing, and texture*

General Terms: Algorithms, Theory, Measurement

Additional Key Words and Phrases: Material appearance, fading, time-dependent phenomena

Fig. 1. Rendering of a newspaper as it turns yellow due to extended light exposure. Model and textures used with permission of Turbosquid [2006; 2010]. Top Left: Before exposure. Top Right: After exposure. Bottom: The newspaper has been unfolded.

1. INTRODUCTION

Computer generated images usually depict settings devoid of signs of wear and tear. The appearance of real-world materials, however, varies over time due a myriad of aging and weathering phenomena. Arguably light exposure is among the main environmental factors responsible for such time-dependent variations. A few examples of material appearance changes caused by light exposure are depicted in Figure 2. For instance, a corkboard may fade in areas where it is exposed to sunlight from a nearby window. This fading may be lacking in areas that were once covered with photographs or posters. A painting on a wall may lose some of its colors after being excessively exposed to light, with some colors fading more readily than others. Accounting for these effects provides the viewer with important visual cues, significantly improving the perceived realism of a given scene.

In this article, we introduce a novel theoretical framework for the analysis and simulation of material appearance changes over time due to light exposure. This framework is based on the general formulation for light transport within a medium [Arvo 1993]. It employs a physicochemical approach that accounts for the kinetics of pigment and dye fading processes as well as variations in exposure

Fig. 2. Photographs depicting scenes in which fading due to light exposure has taken place. Top Left: An area rug has faded everywhere except where a couch had been placed. Top Right: A newspaper has turned yellow from many years of light exposure. Middle: Printed materials have been added and removed from a bulletin board over time, resulting in an irregular fading pattern. Bottom: The left end of a mural has been exposed to more light than the right, yielding uneven fading along its length. Photographs of the two ends are shown adjacent to one another so that the difference is clearly visible.

level with depth in samples of arbitrary thickness. We describe in detail the application of this framework using the Kubelka-Munk (K-M) theory [Kubelka and Munk 1931], and evaluate its fidelity through comparisons of measured and simulated reflectance curves resulting from different periods of fading. We also illustrate the effectiveness of the model derived from this framework through the rendering of scenes depicting material appearance changes over time.

Besides the contribution to realistic image synthesis, the physically based simulation of fading effects described here has also important cultural and industrial applications. For example, museums are interested in the long-term effects of light exposure on their art collections [Imai et al. 2001; Thomson 2002]. Hence, a compromise must be reached that minimizes damage caused by light exposure, while still allowing enough light for public viewing. In this context, damage caused by visible light is of primary concern, as ultraviolet light may usually be filtered out without affecting viewing by means of a glass case. By taking a physicochemical approach, the proposed framework is able to simulate the fading of objects under experimental and hypothetical conditions. This would allow a conservator to evaluate the use of various filters, coverings, illumination conditions and lighting policies. In the multi-billion dollar

manufacturing sector, one is interested in extending the life of surface finishes such as paints and stains [Hunger and Wilker 2004]. Accordingly, in recent years, substantial research efforts [Learner et al. 2008] have been directed toward this goal. Viewed in this context, a framework for simulating the long-term effects of light exposure can be used by industry researchers to determine how various additives or varnishes affect the lightfastness of surface finishes, that is, their resistance to alterations on light exposure. These investigations, in turn, would allow for the manufacturing of products that can maintain their original colors for longer periods of time.

2. RELATED WORK

Aging and Weathering. While there have been many recent advances toward the modeling of aging and weathering phenomena in computer graphics, the work presented here is the first to address the physically based simulation of light exposure effects on material appearance over time. For in-depth surveys on the modeling of aging and weathering phenomena, the reader is referred to the comprehensive texts by Dorsey et al. [2008] or Mérillou and Ghazanfarpour [2008]. In the following, we present an overview of relevant techniques used to render aging and weathering effects. For the purpose of this overview, we loosely divided these techniques into two groups: phenomenological and functional.

Phenomenological techniques are targeted toward particular effects. For example, Dorsey and Hanrahan [1996] applied erosion and deposition to a layered model in order to simulate and render metallic patinas, while Dorsey et al. [1996] simulated water flow over a surface using particle systems to account for the transport of material and the resulting aged appearance. More recently, Chen et al. [2005] extended this idea by allowing weathering particles to leave the surface by reflection (as in photon transport), and by bouncing off a surface, in addition to flowing along a surface. They also employed the results of their weathering transport computation to render other types of weathering phenomena besides those involving transport of material by water. Bosch et al. [2011] developed techniques for determining flow simulation parameters from images. Kider et al. [2011] used a biologically motivated reaction-diffusion approach to simulate the deterioration of fruit.

Functional techniques are more broadly applicable, but require prior acquisition of the time-varying BRDF data describing the desired effect. For example, Gu et al. [2006] developed a database of the time-varying appearance of materials undergoing various natural processes such as drying or corrosion. This is expressed in the form of a seven dimensional Time and Spatially-Varying BRDF (TSV-BRDF). They described a procedure for factoring the TSV-BRDF into temporally and spatially varying components which may then be stored compactly in their database. Similarly, Wang et al. [2006] noted that the spatially varying appearance of a weathered material, for example rust forming on a sheet of metal, typically reflects variation in the degree of weathering. From spatially variant BRDF data captured from a weathered material sample at a single instant in time, they organized the variety of appearances present in a particular weathering process into an appearance manifold. This manifold was then used to synthesize new textures of the same material representing its weathered appearance at different points in time.

Fading. The relevant work on fading and lightfastness of materials comes primarily from the conservation field. Giles and McKay [1963] and Giles [1965] studied the factors and mechanisms that contribute to fading of dyes and pigments. They found

that a finely dispersed dye would fade more readily than one in an aggregate form. Johnston-Feller et al. [1984] studied the fading rates of thin films of several pigments under various levels of exposure. They observed that the fading behavior followed first-order kinetics, that is, the rate at which pigment is lost over time is proportional to its concentration. The formulation of our framework is consistent with these findings. In addition, it accounts for a wide range of variations in the light exposure and sample conditions.

Whitmore and Bailie [1997] developed a mathematical model to describe the fading of transparent glazes. Their model was limited to nonscattering media subjected to monochromatic illumination. These simplifications allowed them to consider the medium as a whole without accounting for the variation in fading with depth. Our proposed framework removes these limitations.

Morris and Whitmore [2007] extrapolated the results of micro-fading tests to visualize the faded appearance of an entire painting or museum object. Small areas (approximately $0.4\,mm^2$) of the object were faded with intense illumination while the color was continuously measured to produce a fading curve in CIE Lab space [Whitmore et al. 1999]. The results of these micro-fading tests were extrapolated to visualize the entire object after years of light exposure [Morris and Whitmore 2007]. While this approach may correctly predict the fading of other areas of the object having the same properties as the measured sample, it is unclear how it can correctly predict the fading rate of areas with different properties (e.g., distinct pigment composition). In addition, this data-driven approach is limited to simulating the rate of fading of the material measured under the specific illumination used in the test. In contrast, the comprehensive physicochemical approach employed in our framework allows us to perform not only data-driven, but also theoretical fading simulations involving materials with different properties and subject to a wide range of illumination conditions.

Shi et al. [2006] and Shi and Lu [2005] used per-pixel spline interpolation in the RGB color space in order to visualize the appearance of fading works of art at intermediate stages. The initial and final results of the fading processes are required as input. This is not always feasible, particularly when the processes involved take place over extended periods of time. In addition, it is worth noting that this technique was not designed to predict how fading may evolve under hypothetical circumstances.

Berns [2005] and Berns et al. [2005] have proposed techniques for digital restoration of paintings. The spectral properties of the degraded pigments and of the corresponding undegraded pigments are measured. Intermediate stages are simulated as a mixture of these two extremes using single-constant Kubelka-Munk theory.

Applications of Kubelka-Munk Theory. The theory for light transport in a uniform medium proposed by Kubelka and Munk [1931] has been extended and successfully employed in a wide assortment of disciplines to simulate light interactions with various man-made and natural materials, from plastics [Saunderson 1942] and printer inks [Yang 2003] to plants [Seyfried and Fukshansky 1983] and human skin [Doi and Tominaga 2003]. In conservation, Johnston-Feller [2001] employed the K-M theory to account for the effects of light exposure on museum objects using empirical techniques. In computer graphics, Haase and Meyer [1992] applied the K-M theory to facilitate correct-color calculations for realistic image synthesis. Subsequently, this theory has been employed in the rendering of artistic effects involving painting media such as watercolors [Curtis et al. 1997] and wax crayons [Rudolf et al. 2003]). It has also been used as a component in more complex models. For example, Dorsey and Hanrahan [1996] simulate natural processes, such as erosion and deposition, in a layered model based on the

earlier work of Hanrahan and Krueger [1993] to achieve the appearance of a metallic patina. They used K-M theory to account for the scattering and absorption within each layer. Abdul-Rahman and Chen [2005] employed the K-M theory to propose a spectral volume rendering technique that more accurately accounts for absorption and scattering properties than simple alpha blending in RGBA space. More recently, Hašan et al. [2010] incorporated the K-M theory in their work aimed at fabricating objects with predetermined subsurface scattering properties.

Yellowing. Paper that has not been chemically treated turns yellow during prolonged exposure to daylight, and ultraviolet light in particular [Heitner 1993]. This process is called *brightness reversion*. Brightness reversion occurs as lignin, which accounts for 17-35% by weight of the wood used in paper production [Roberts 1996], undergoes a photochemical reaction resulting in the formation of yellow chromophores known as *orthoquinones* [Heitner 1993]. Heitner [1993] outlines the development of current understanding of the reaction pathways involved in paper yellowing. To the best of our knowledge, this phenomenon has not been specifically addressed in the computer graphics literature before.

3. THEORETICAL FRAMEWORK

The goal of the proposed framework is to account for the light induced changes in material appearance as time progresses. In particular, we consider spectral changes such as the fading of pigments and dyes or the light induced yellowing of paper.

These changes in appearance require that a chemical reaction takes place within the material [Giles and McKay 1963]. To compute the effect of light exposure therefore requires that we understand the subsurface light environment. Furthermore, conservation of energy dictates that, in the case of light induced fading, absorption takes place in order to initiate a reaction. This is known as the Grotthus–Draper law [Giles and McKay 1963]. The induced changes in material properties within the subsurface volume are then accumulated over time.

In the following, we describe the theoretical underpinnings of our framework. Using the scattering model proposed by Kubelka and Munk [1931], we examine in detail the application of the proposed framework to the two-flux scenario. In Section 3.3, we describe how the proposed framework may be generalized to account for arbitrary light environments. The symbols used in the following derivations are summarized in Table I.

3.1 Uniform Slab

In this section, we consider the case of a uniform slab of absorbing and scattering material subjected to collimated illumination from above. We shall employ the two-flux approach similar to the theory originally proposed by Kubelka and Munk [1931]. Since, in this section, we are considering radiation in the vertical directions only, all quantities vary only in the direction of the z-axis.

Let E^d indicate the downwelling flux density and E^u indicate the upwelling flux density. After traversing a unit distance dz, E^d is diminished due to absorption by $\mu^a E^d\,dz$, due to outscattering by $\mu^s E^d\,dz$, and augmented due to inscattering by $\mu^s E^u\,dz$. The upwelling flux density E^u is diminished and augmented in a similar manner, yielding the following system of differential equations

$$E_z^d = -(\mu^a + \mu^s)E^d + \mu^s E^u, \qquad (1)$$

$$-E_z^u = -(\mu^a + \mu^s)E^u + \mu^s E^d, \qquad (2)$$

Table I. Symbols Used in This Article

Symbol	Description	Units
Z	depth	m
ρ	reflectance	
τ	transmittance	
L	radiance	$\mathrm{W\,m^{-2}\,sr^{-1}}$
L_e	emitted radiance	$\mathrm{W\,m^{-2}\,sr^{-1}}$
μ	attenuation coefficient	$\mathrm{m^{-1}}$
μ^a	absorption coefficient	$\mathrm{m^{-1}}$
μ^s	scattering coefficient	$\mathrm{m^{-1}}$
σ_g	cross section / total volume	$\mathrm{m^{-1}}$
σ_p	cross section / particle volume	$\mathrm{m^{-1}}$
α^a	absorption efficiency	
α^s	scattering efficiency	
f	volume fraction	
β	volumetric fading rate	$\mathrm{m^3\,J^{-1}}$
γ	volumetric breakdown rate	$\mathrm{m^3\,J^{-1}}$
Φ	fluence	$\mathrm{J\,m^{-2}}$
F	fluence rate	$\mathrm{W\,m^{-2}}$
F_λ	spectral fluence rate	$\mathrm{W\,m^{-2}\,nm^{-1}}$
E	irradiance	$\mathrm{W\,m^{-2}}$
$\mathbf{E}$	irradiance vector	$\mathrm{W\,m^{-2}}$
$\mathcal{S}^2$	unit sphere	
E^u	upward irradiance	$\mathrm{W\,m^{-2}}$
E^d	downward irradiance	$\mathrm{W\,m^{-2}}$
ρ^*	ground reflectance	
$\mathbf{E}^u$	upward irradiance vector	$\mathrm{W\,m^{-2}}$
$\mathbf{E}^d$	downward irradiance vector	$\mathrm{W\,m^{-2}}$
$\mathbf{T}$	downward transmission matrix	
$\mathbf{R}^\wedge$	downward reflection matrix	
$\mathbf{R}^\vee$	upward reflection matrix	
$\mathbf{M}$	transfer matrix	
$\mathbf{R}$	reflection submatrix	
$\mathbf{T}^u$	upward transmission submatrix	
$\mathbf{T}^d$	downward transmission submatrix	
$\mathbf{I}$	identity matrix	

where E_z^d and E_z^u denote the partial derivatives of E^d and E^u with respect to the depth z.

To account for the effects of light exposure over time, we first introduce time as a parameter to all components of Eqs. (1) and (2): E^u, E^d, μ^a and μ^s. Differential equations must then be derived to describe how $\mu^a(z, t)$ and $\mu^s(z, t)$ vary with light exposure over a period of time. The resulting system of differential equations that includes Eqs. (1), (2), and these additional differential equations describing the effects of light exposure, must then be solved. Typically, to obtain a solution, it will be necessary to use numerical methods. These methods will be discussed in Section 4.

The local light environment within the medium is described by the *fluence rate*, which is defined as

$$F(\vec{r}) = \int_{\mathcal{S}^2} L(\vec{r}, \omega)\, d\omega, \tag{3}$$

where $L(\vec{r}, \omega)$ denotes the radiance at position $\vec{r}$ in the direction $\omega = (\theta, \phi)$. The absorbed energy density at a given point within the medium is the product of the *fluence*, $\Phi = F\, dt$, and the absorption coefficient, μ^a [Grossweiner et al. 2005]. We define β, in $\mathrm{m^3\,J^{-1}}$, as the volume of particulate matter consumed by a given amount of energy. This is consistent with prior observations found in the conservation literature [Morton 1949]. The local change in

the volumetric concentration, f, of the colorant is then given by

$$df = -\beta \mu^a F\, dt. \tag{4}$$

Combining Eqs. (1), (2) and (4), we are then left with the following system of differential equations

$$E_z^d = -(\mu^a + \mu^s)E^d + \mu^s E^u, \tag{5}$$

$$-E_z^u = -(\mu^a + \mu^s)E^u + \mu^s E^d, \tag{6}$$

$$f_t = -\beta \mu^a F. \tag{7}$$

Additionally, we have the boundary conditions

$$\mu^a(z, 0) = \mu_0^a, \tag{8}$$

$$\mu^s(z, 0) = \mu_0^s, \tag{9}$$

$$E^d(0, t) = E_0, \tag{10}$$

$$E^u(z_{\max}, t) = \rho^* E^d(z_{\max}, t), \tag{11}$$

where μ_0^a and μ_0^s are the initial absorption and scattering coefficients of the medium, respectively, E_0 is the irradiance of the collimated illumination from above, $z_{\max}$ is the depth of the medium, and ρ^* is the reflectance of the substrate.

3.1.1 *Mixtures.* In this section, we examine a colorant consisting of a mixture of component substances (pigments or dyes). Let the absorption and scattering coefficients be given by μ_j^a and μ_j^s, respectively. The absorption and scattering components of the mixture are then

$$\mu^a = \sum_j \mu_j^a, \tag{12}$$

$$\mu^s = \sum_j \mu_j^s. \tag{13}$$

The absorption and scattering coefficients of the mixture are used to determine how F varies with depth, z, following the same procedure as before. However, the reduction in the volume fraction occupied by each single colorant is proportional to the energy absorbed by this particular colorant. Thus, $df_j = -\beta_j \mu_j^a F\, dt$ for $j = 1, \ldots, m$.

Note from Eq. (7) that any colorant that does not absorb (i.e., $\mu^a = 0$) will not fade. This is consistent with the law of conservation of energy. If a medium consists of a mixture where some components scatter but do not absorb, and the remainder absorb but do not scatter, then the scattering components will not fade. Consequently, the scattering will be left unaffected by light exposure. In this scenario, we consider μ^s as constant.

3.1.2 *Spectral Considerations.* In the multispectral context, the reduction in the volume fraction of a colorant is proportional to the energy absorbed by that colorant across the entire spectrum. That is,

$$df_j = -dt \int_0^{\lambda_{\max}} \beta_j \mu_j^a F_\lambda\, d\lambda. \tag{14}$$

Here, the absorption coefficients μ_j^a become wavelength dependent and the fluence rate is substituted by the *spectral fluence rate*, F_λ (having units of $\mathrm{W\,m^{-2}\,nm^{-1}}$). The volumetric fading rate β_j is proportional to the number of photons absorbed, and is therefore linearly proportional to the wavelength [Rånby and Rabek 1975]. For fading to occur, the photon energy must be sufficient to cause excitation. The wavelength must therefore be less than some maximum wavelength $\lambda_{\max}$.

3.2 Nontrivial Breakdown Products

In some cases, the breakdown products of a light-dependent reaction may not be colorless. For instance, some papers develop a yellow in hue after exposure to ultraviolet light. This may be attributed to the formation of orthoquinones when the lignin is irradiated with UV light [Heitner 1993]. To account for this, we add a positive term to the equations to the system to model the increase in these breakdown products due to light absorption

$$df_j = -\beta_j \mu_j^a F\, dt + \sum_{i \neq j} \gamma_{i,j} \mu_i^a F\, dt. \tag{15}$$

for $j = 0, \ldots, m$, where $\gamma_{i,j}$ denotes the rate at which constituent i breaks down into constituent j due to light absorption by i. If only a single constituent breaks down into j, then only a single term in the preceding summation will be nonzero.

3.3 Generalization to Arbitrary Light Environments

To describe the light environment below the surface of the material to be subjected to light exposure over time, we begin with the general equation for light transport in three-dimensional space [Arvo 1993]

$$\omega \cdot \nabla L(\mathbf{r}, \omega) + \mu(\mathbf{r}) L(\mathbf{r}, \omega)$$
$$= L_e(\mathbf{r}, \omega) + \int_{\mathcal{S}^2} k(\mathbf{r}; \omega' \cdot \omega) L(\mathbf{r}, \omega')\, d\omega', \tag{16}$$

where $\mu = \mu^a + \mu^s$ is the attenuation coefficient, L_e is the emitted radiance, and k represents the volume scattering kernel. Eq. (16) indicates that the radiance along a path is reduced by absorption and outscattering, and increased by emission and inscattering. Scattering and absorption are accounted for everywhere in three-dimensional space, thereby handling participating media and subsurface scattering in a natural way.

As indicated, we introduce time as a parameter to all components of Eq. (16) and determine the differential equations that describe how μ and k vary with light exposure over a period of time. As before, light exposure is expressed in terms of the fluence rate, given in this case by

$$F(\mathbf{r}) = \int_{\mathcal{S}^2} L(\mathbf{r}, \omega)\, d\omega. \tag{17}$$

Note that the two-flux case may be expressed as a special case of Eqs. (16) and (17) by letting

$$L(z, \omega) = E^d(z)\delta(\omega, \mathbf{k}) + E^u(z)\delta(\omega, -\mathbf{k}), \tag{18}$$
$$\mu(z) = \mu^a + \mu^s, \tag{19}$$
$$L_e(z, \omega) = E_0\delta(z)\delta(\omega, \mathbf{k}), \tag{20}$$
$$k(z; \omega' \cdot \omega) = \mu^s\delta(\omega' \cdot \omega + 1), \tag{21}$$

where $\delta(x)$ represents the Dirac delta function, and we define $\delta(\omega_1, \omega_2) = \delta(\cos\theta_1 - \cos\theta_2)\delta(\phi_1 - \phi_2)$.

4. NUMERICAL APPROACHES

To the best of our knowledge, the system of Eqs. (5)–(11) has no closed-form solution [Polyanin and Zaitsev 2004]. We must therefore resort to numerical methods. To accomplish this task, we first discretize the domain in the vertical depth (z) and the time (t) dimensions. We then solve the problem in each dimension in turn, holding μ^a and μ^s constant within each interval. We have used uniform depth and time intervals in our analysis for simplicity,
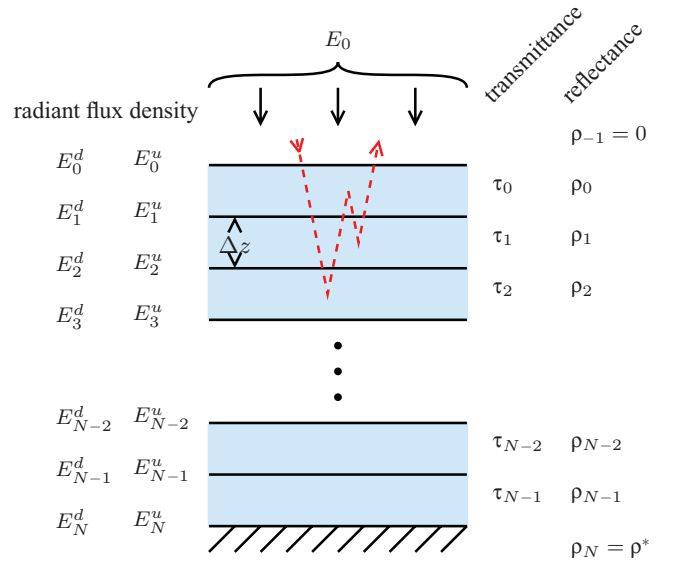

Fig. 3. Diagram depicting the vertical discretization of the simulated medium according to the two-flux model. The thickness of each layer is denoted by Δz. Each layer is uniform in its absorption and scattering, from which the reflectance and transmittance of the layer in isolation, as indicated on the right, may be computed using the K-M theory [Kubelka 1948]. From these quantities, the radiant flux density at the layer boundaries, shown on the left, may be determined. The dashed line schematically describes a sample path through the medium.

although arbitrary discretization strategies may be employed. Extending the following to allow for variable depth and/or time steps is straightforward.

4.1 Depth Discretization Step

To solve for the radiant flux densities E^d and E^u at a fixed time, we discretize along the z-axis into N layers and hold μ^a and μ^s constant within each layer as depicted in Figure 3. Under these assumptions, the reflectance and transmittance of each layer may be computed using Kubelka's formulae for a finite layer [Kubelka 1948]

$$\rho_i = \frac{1}{a_i + b_i \coth b_i \mu_i^s \Delta z}, \tag{22}$$
$$\tau_i = \frac{b_i}{a_i \sinh b_i \mu_i^s \Delta z + b_i \cosh b_i \mu_i^s \Delta z}, \tag{23}$$

where $a_i = (\mu_i^s + \mu_i^a)/\mu_i^s$ and $b_i = \sqrt{a_i^2 - 1}$. Since each layer has uniform scattering and absorption properties throughout, the reflectance and transmittance of each layer is the same from below as from above. Note also that Eq. (22) uses a ground reflection of zero. This equation therefore only accounts for reflection within layer i and not for reflection due to subsequent transmission through layer i after reflection from another layer or from the ground. Additionally, we define $\rho_{-1} = 0$ to be the reflectance of the infinite, nonscattering top layer and $\rho_N = \rho^*$ to be the ground reflectance.

Let $E_i^d = E^d(i\Delta z)$, $E_i^u = E^u(i\Delta z)$, for $0 \leq i \leq N$. These values may be expressed in terms of the reflectances and transmittances of

the layers using the following system of equations.

$$E_0^d = E_0 \tag{24}$$

$$E_i^u = \rho_i E_i^d + \tau_i E_{i+1}^u \qquad 0 \le i < N \tag{25}$$

$$E_i^d = \tau_{i-1} E_{i-1}^d + \rho_{i-1} E_i^u \qquad 0 < i \le N \tag{26}$$

$$E_N^u = \rho_N E_N^d \tag{27}$$

This may be expressed in matrix form as

$$\mathbf{E} = \mathbf{ME} + \mathbf{E}_0, \tag{28}$$

where $\mathbf{E}$ and $\mathbf{E}_0$ are $2(N+1)$-dimensional vectors given by

$$\mathbf{E} = \left(E_0^u, E_0^d, \dots, E_N^u, E_N^d \right)^T, \tag{29}$$

$$\mathbf{E}_0 = (0, E_0, 0, \dots, 0)^T, \tag{30}$$

and $\mathbf{M}$ is a $2(N+1) \times 2(N+1)$ block tridiagonal matrix

$$\mathbf{M} = \begin{pmatrix} \mathbf{R}_0 & \mathbf{T}_0^u & & 0 \\ \mathbf{T}_0^d & \ddots & \ddots & \\ & \ddots & \ddots & \mathbf{T}_{N-1}^u \\ 0 & & \mathbf{T}_{N-1}^d & \mathbf{R}_N \end{pmatrix} \tag{31}$$

having 2×2 blocks

$$\mathbf{R}_i = \begin{pmatrix} 0 & \rho_i \\ \rho_{i-1} & 0 \end{pmatrix} \qquad 0 \le i \le N, \tag{32}$$

$$\mathbf{T}_i^u = \begin{pmatrix} \tau_i & 0 \\ 0 & 0 \end{pmatrix} \qquad 0 \le i < N, \tag{33}$$

$$\mathbf{T}_i^d = \begin{pmatrix} 0 & 0 \\ 0 & \tau_i \end{pmatrix} \qquad 0 \le i < N. \tag{34}$$

The block tridiagonal structure of this system allows for it to be solved in $O(N)$ time [Isaacson and Keller 1994], rather than the $O(N^3)$ time required for a general system of linear equations.

—*Fluence Rate Estimation.* The fluence rates at the layer boundaries are given by $\mathbf{F} = \mathbf{E}^d + \mathbf{E}^u$. The mean fluence rate within layer i is estimated by taking the average of the fluence rates at the boundaries.

$$F_i = \frac{1}{2} (\mathbf{F}_i + \mathbf{F}_{i+1})$$

We remark that the spectral fluence rate F_λ may be computed independently for each wavelength.

4.2 Time Stepping

Time stepping proceeds by solving Eq. (14) while holding the fluence rate constant within each layer. The absorption coefficients are then updated according to

$$f(t + \Delta t) = f(t) \exp \left(-\Delta t \int_0^\infty \beta \mu^a F_\lambda \, d\lambda \right). \tag{35}$$

The spectral fluence rate F_λ is computed for a fixed set of wavelengths using the procedure described in the previous section. The absorption coefficient μ^a is sampled at the same set of wavelengths. The result is then integrated numerically. Finally, the absorption coefficient may be updated according to

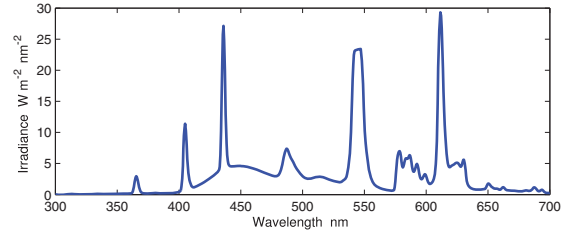$$\mu^a(t + \Delta t) = \frac{f(t + \Delta t)}{f(t)} \mu^a(t). \tag{36}$$

Fig. 4. Spectral irradiance of the 27 W fluorescent light bulb used in the experiments as measured from 5/8" from the center of the bulb (the distance from which the samples were illuminated).
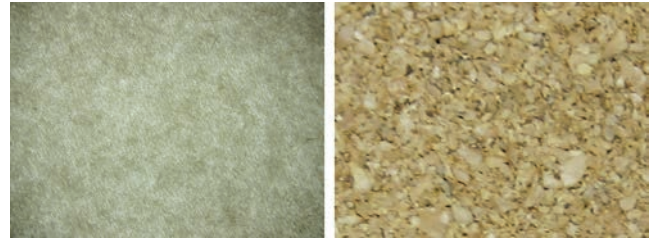

Fig. 5. Photographs depicting the heterogeneous structure of the materials used in the experiments: Left: newsprint, Right: cork.

5. EVALUATION PROCEDURES

In this section, we describe our evaluation approach in which we compare measured and simulated reflectance curves obtained as fading takes place over an extended period of time. Several sets of experiments were conducted subjecting various materials to light exposure over time. The materials selected for experimentation included 30 lb (48.8 g m^{-2}) newsprint paper (70 μm thick), two dyes (Toluidine Blue O and Congo Red), and a fine-grain cork (typically used for bulletin boards). Square samples were prepared and affixed to a piece of bristol board with two-sided tape around the edges of each sample to prevent them from curling during exposure, thus maintaining a consistent distance and orientation with respect to the light source.

The samples were exposed to light from a 27 W fluorescent bulb. This type of lamp was selected to minimize the effects of heat as a cause of fading. The spectral power distribution of the bulb is depicted in Figure 4.

Reflectance measurements were taken before exposure, after every six hours of exposure up to twenty-four hours, and after every twenty-four hours thereafter up to seven days. Measurements were performed using a StellarNet Inc. BLK-C-SR spectrophotometer with a SL1-Filter Tungsten/Krypton lamp. Although the measured values presented some quantitative variability due to the handling of heterogeneous sample materials (Figure 5), the dominant spectral trends in the progression of reflectance curves were fully preserved. This is an essential evaluation requisite since the main purpose of these experiments was to provide spectral references for assessing whether the proposed framework can capture different fading behaviors.

5.1 Paper

Reflectance measurements over black and over white substrates were taken of the unexposed sample in order to determine separately the initial scattering and absorption coefficients of the newsprint, depicted in Figure 6, using the method described in Appendix A.
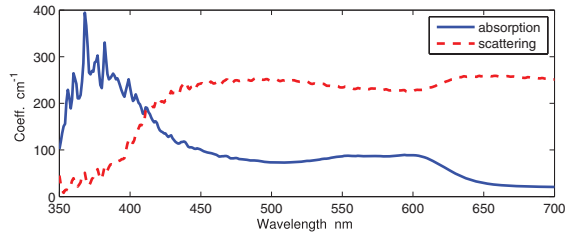
Fig. 6.   Scattering and absorption coefficients of the newsprint used in our experiments.
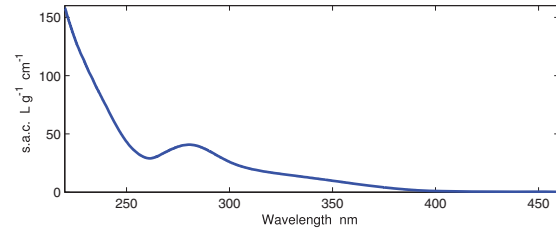

Fig. 7.   Specific absorption coefficient (s.a.c.) of lignin [Glading 1940].
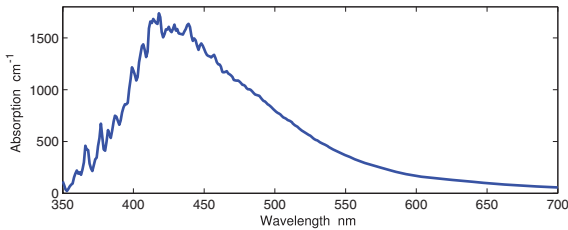

Fig. 8.   Absorption coefficient of the fully yellowed newsprint used in our experiments.

The initial absorption coefficient was separated into a component for lignin and a component for the remaining constituents. The lignin content of newsprint is similar to that of the wood from which it was produced, which typically falls in the range of 20-27% [Roberts 1996]. The midpoint of this range was used in our simulations. The specific absorption coefficient of lignin [Glading 1940] is shown in Figure 7 (left). Further, it was assumed that absorption by lignin produced a chromatic breakdown product, whereas other substances broke down to a nonabsorbing material. The absorption coefficient of the breakdown products resulting from absorption by lignin was determined by exposing a sample of newsprint on both sides for long enough to allow the sample to completely yellow. The absorption coefficient was then computed from the reflectance measurement under the assumption that the scattering coefficient was unaffected (Figure 8).

5.2   Dyes

Solutions of the dyes (Toluidine Blue O and Congo Red) in water were prepared in test tubes. Squares of newsprint paper were cut. Samples were prepared for each solution by pouring the solution into a petri dish and soaking one of the squares until the solution penetrated the paper. The samples were hung vertically in a dark environment to dry. Since the pigmented samples were too dark to allow for incomplete hiding of the substrate, we have assumed that the pigments themselves contribute only to absorption, eliminating
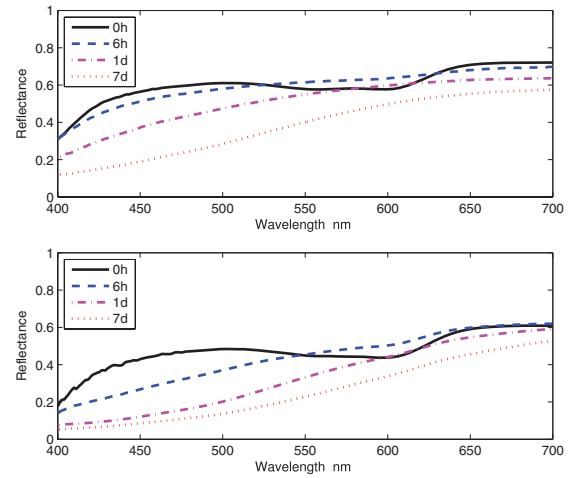

Fig. 9.   Measured and simulated reflectances of yellowing newsprint as obtained from the front (illuminated) side of the paper initially (0h) and after six hours (6h), one day (1d), and seven days (7d). Top: Measured progression of reflectance curves. Bottom: Simulated progression of reflectance curves.

the requirement for separate reflectance measurements over black and over white substrates.

5.3   Cork

A $1/32$" (0.8 mm) thick sample of fine-grain cork was used. Due to the infeasability of obtaining a cork sample thin enough for reflectance measurements with incomplete hiding, only a single reflectance measurement was taken before light exposure and after each time interval. Thus, only the ratio of the absorption and scattering coefficients may be obtained. In our simulations, we used the average specific scattering coefficient over the visible region of the spectrum measured from the newsprint ($237\,\mathrm{L\,g^{-1}\,cm^{-1}}$) as an approximation of the scattering from cork. Cork contains approximately 22.7% lignin by weight [Pereira 2007]. The absorption coefficient used was therefore expressed as a sum of the absorption coefficient for this concentration of lignin and the remaining constituents, which were assumed to break down into a colorless product.

6.   RESULTS AND DISCUSSION

Section 6.1 discusses the results of the experiments described in Section 5. Section 6.2 discusses the behavior of the framework and draws comparisons with the literature. In Section 6.3, we present several scenes rendered to further illustrate the applicability of our framework in realistic image synthesis.

6.1   Experimental Results

Figure 9 shows the measured (top) and simulated (bottom) reflectance curves obtained from the illuminated side of the newsprint before exposure and after several periods of exposure to light from the fluorescent lamp. For clarity, we have selected a representative set of curves to show in the plots. Note that our framework is able to capture the simultaneous rapid fading of the absorption band between 500 and 600 nm and the darkening caused by yellowing of the lignin. We remark that the difference in the absolute level of the measured versus simulated initial reflectance curves is attributable to the spatial variation in the internal structure of the newsprint, as

Table II. Fading Rates Used in the Experiments

Material	β (at 400 nm)	$\lambda_{\max}$
Lignin	1.670×10^{-9}	400 nm
Newsprint[*]	1.002×10^{-8}	700 nm
Cork[*]	2.000×10^{-13}	700 nm
Toluidine Blue O	1.336×10^{-13}	700 nm
Congo Red	1.336×10^{-13}	700 nm

[*] considering constituents other than lignin.

Table III. Breakdown Rate Used in the Experiments for Newsprint and for Cork.

From Material	To Material	γ (at 400 nm)	$\lambda_{\max}$
Lignin	o-Quinone	1.670×10^{-9}	400 nm

Table IV. Time Required (in seconds) to Simulate The Effect of Light Exposure on Newsprint Using the Proposed Framework, and Considering 371 Wavelengths (330-700 nm at 1 nm intervals)

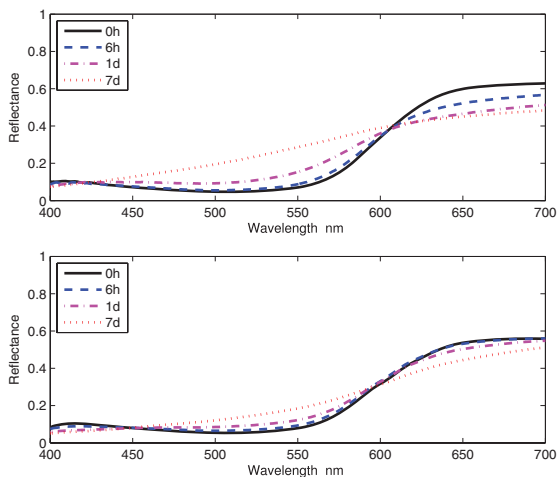| No. of Layers	Time Steps				
	20	40	60	80	100
10	3.66	7.31	10.96	14.62	18.27
100	6.84	13.66	20.49	27.32	34.15
1000	41.38	82.87	124.19	165.51	206.73

Fig. 10. Measured and simulated reflectances of newsprint dyed with Congo Red as obtained from the front (illuminated) side of the sample initially (0h) and after six hours (6h), one day (1d), and seven days (7d). Top: Measured progression of reflectance curves. Bottom: Simulated progression of reflectance curves.

shown in Figure 5 (left). The fading parameters used are given in Tables II and III.

Table IV shows timings for simulating the yellowing of newsprint on a single core of a machine with two 2.8 GHz quad core Xeon processors. Timings for other simulations were similar.

Figure 10 shows the measured (top) and simulated (bottom) reflectance curves obtained from the front side of the newsprint dyed with Congo Red prior to exposure and after several periods of exposure to light from the fluorescent lamp. Note that the pivot point at approximately 600 nm produced by the simultaneous fading of the Congo Red dye and the yellowing of the newsprint is reproduced by our framework.
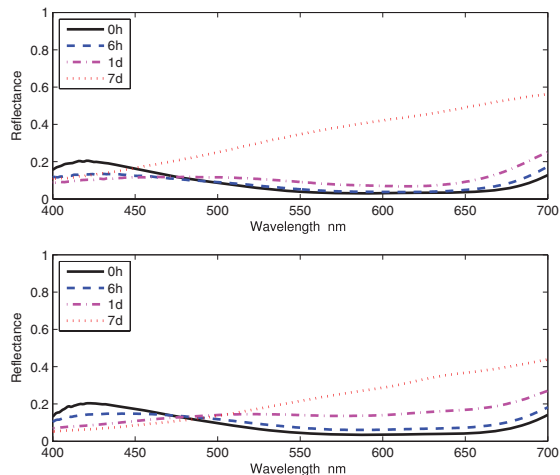
Fig. 11. Measured and simulated reflectances of newsprint dyed with Toluidine Blue O as obtained from the front (illuminated) side of the sample initially (0h) and after six hours (6h), one day (1d), and seven days (7d). Top: Measured progression of reflectance curves. Bottom: Simulated progression of reflectance curves.
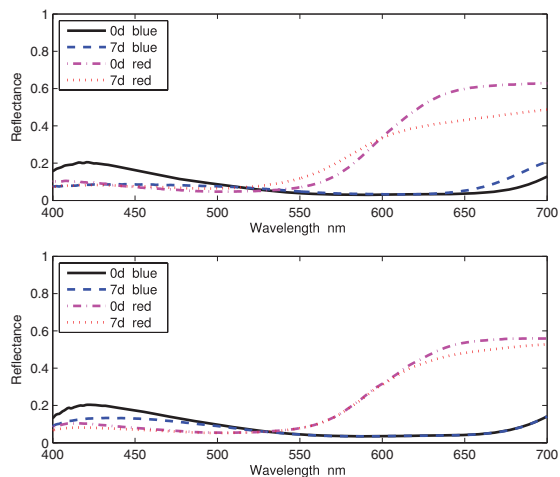

Fig. 12. Measured and simulated reflectances of newsprint dyed with Toluidine Blue O (blue) and Congo Red (red) as obtained from the back (unilluminated) side of the sample initially (0d) and after seven days (7d). Top: Measured reflectance curves. Bottom: Simulated reflectance curves.

Figure 11 shows the measured (top) and simulated (bottom) reflectance curves obtained from the front side of the newsprint dyed with Toluidine Blue O. Note that the pivot point in the blue end of the visible spectrum is reproduced in our simulation. This is caused by the simultaneous fading of the Toluidine Blue O dye with the yellowing of the newsprint.

Figure 12 depicts the corresponding reflectance curves obtained from the back of the dyed newsprint samples. Note that our framework can also reproduce the preferential darkening on the red end of the spectrum on the unexposed side of the newsprint dyed with Congo Red. This is caused primarily by the spike in the spectral irradiance from the lamp in the near ultraviolet at approximately 370 nm (see Figure 4). In this region, the Congo Red dye absorbs very little, allowing this light to penetrate through the paper and
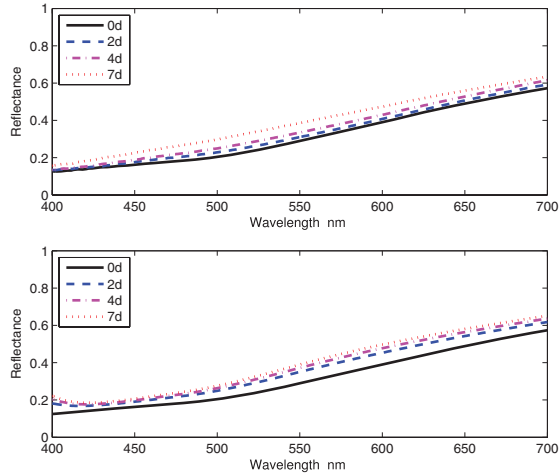
Fig. 13. Measured and simulated reflectance curves of fading cork initially and after six hours, one day, and seven days. Top: Measured progression of reflectance curves. Bottom: Simulated progression of reflectance curves.
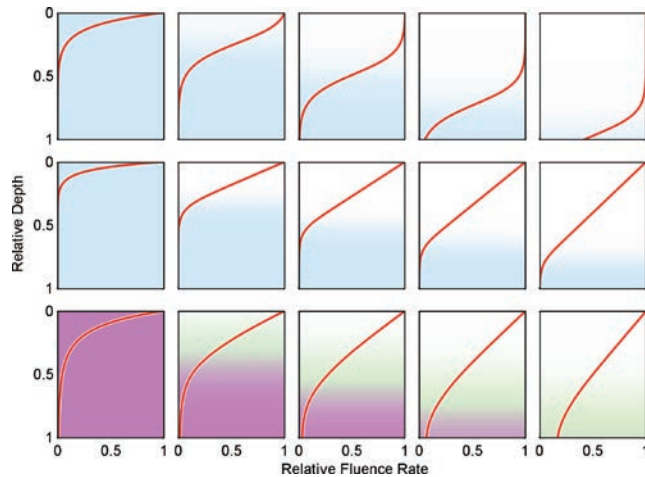

Fig. 14. Sequences of plots depicting the progression of fading as simulated by the proposed framework. The shading denotes the value of the absorption coefficient, relative to its original value. The red line indicates the fluence rate, relative to the fluence rate at the surface. Top Row: Fading of a non-scattering sample. The colorant is consumed at a constant rate, progressing downward over time. Middle Row: Fading of a highly scattering sample. The rate at which the colorant is consumed decreases with time. Bottom Row: Fading of a mixture of pigments of varying lightfastness. The hue of the shaded area represents the relative volume fraction of the component colorants with depth.

cause yellowing through to the other side. Since the dye is highly absorbing in the visible region, however, very little light penetrates through the sample and there is therefore no fading seen from the unexposed side. Similarly, note the preferential darkening in the blue end of the spectrum on the unexposed side. This may be explained in a similar manner as with the red sample.

Figure 13 shows the measured and simulated progression of reflectance curves for cork. Note that the reflectance curve maintains its general shape while increasing in value over time. This is caused by the simultaneous yellowing of the lignin with the fading of the

Table V. Sets of Fading Rates Used for the Pigments
Used in the Renderings Depicted in Figure 15

		Pigment	
Row	Cyan	Magenta	Yellow
1	8.661×10^{-8}	9.735×10^{-8}	1.256×10^{-7}
2	8.661×10^{-8}	4.867×10^{-8}	6.279×10^{-8}
3	4.331×10^{-8}	1.217×10^{-7}	6.279×10^{-8}
4	4.331×10^{-8}	4.867×10^{-8}	2.511×10^{-7}

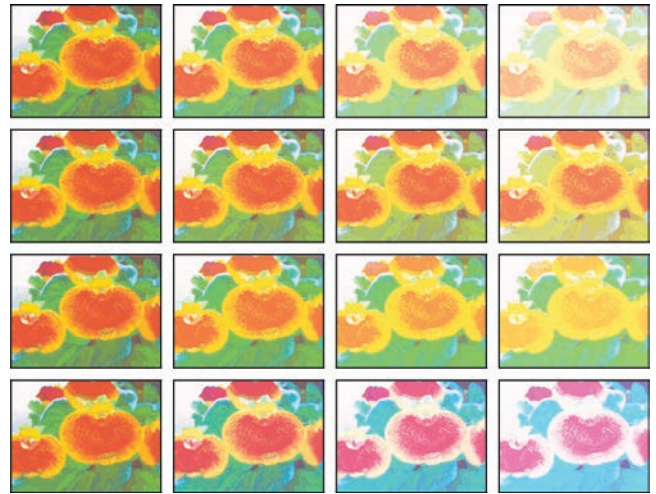The fading rates are quoted in $m^3 \, J^{-1}$ at 500 nm.

Fig. 15. Rendering of an image composed of mixtures of cyan, magenta, and yellow pigments is faded according to four hypothetical sets of fading rates for a total exposure of $4.365 \times 10^7 \, J \, m^{-2}$. The sets of fading rates used are indicated in Table V. Top Row: The pigments fade at perceptually similar rates. Second Row: The cyan pigment fades more rapidly. Third Row: The magenta pigment fades more rapidly. Bottom Row: The yellow pigment fades more rapidly.

remaining constituents. Without yellowing of the lignin, the reflectance curves would flatten out as fading progressed. That is, fading would proceed faster in the blue end of the spectrum than in the red end.

6.2 Phenomenological Assessment

Figure 14 shows the progress of fading under different conditions as simulated by our framework. The top sequence indicates the resulting behavior for a nonscattering medium. In this instance, fading proceeds as a wave of colorant decomposition that progresses downward at a constant rate. This is consistent with prior observations reported in the literature [Giles et al. 1968]. Conversely, for scattering media, the progression of fading slows over time. This behavior is depicted in the middle row of Figure 14, and agrees with the findings of Johnston-Feller [1986] in which the depth of fading decreased with increasing TiO_2 content (a tint). Finally, the bottom sequence depicts the fading of a mixture of pigments in which one of them fades faster than the others. Examples of image sequences rendered using this technique are presented in Figure 15. The corresponding fading rates for each of the components are indicated in Table V. Fading parameters required to obtain 50% fading over a fixed period of time are provided for selected pigment combinations under several lighting conditions in Table VI.

Fig. 16. A living room scene in which the carpet has faded over many years of light exposure. Some models used with permission of Turbosquid [2004; 2007; 2009]. *Left:* Before exposure, *Middle:* After exposure, *Right:* The furniture has been removed, revealing areas that have been masked from fading.

Fig. 17. In a sunroom, a painting (composed of single colorants) has its colors altered after an extended period of light exposure. *Left:* Before exposure, *Middle:* After exposure, *Right:* Closeup of the painting.

Table VI. Fading Rates (in $m^3 J^{-1}$ at 500 nm) Required to Fade Selected Combinations of Pigments by a Factor of 50% (measured according to the luminance of the material relative to the luminance of the unpigmented medium) in Approximately 56 Hours (8 hours per day for 7 days) under Daylight (D65 with a peak irradiance of approximately $1.6\,W\,m^{-2}\,nm^{-1}$) and Incandescent (100 W bulb at a distance of 1 m) Illumination

Pigments	Daylight	Incandescent
Cyan	3.385×10^{-8}	9.128×10^{-6}
Magenta	3.812×10^{-8}	2.354×10^{-5}
Yellow	4.825×10^{-8}	7.753×10^{-5}
Cyan + Magenta	4.817×10^{-8}	2.423×10^{-5}
Cyan + Yellow	4.350×10^{-8}	1.452×10^{-5}
Magenta + Yellow	5.211×10^{-8}	3.393×10^{-5}
Cyan + Magenta + Yellow	6.027×10^{-8}	3.315×10^{-5}

6.3 Rendered Scenes

Figure 1 and Figures 16–18 present images depicting different fading scenarios, before and after extended periods of light exposure. Where artistic effect is the primary motivation, one may employ the monochromatic approach on the individual RGB channels for simplicity. This technique was used in Figures 16 and 17.

Figure 16 shows a typical living room with a fugitive carpet. To determine the mean light exposure incident as a function of position, a Monte Carlo renderer was modified to allow the floor surface to function as a camera. The position and orientation of various pieces of furniture were jittered randomly for each sample to account for the fact that these objects would not maintain their locations over a light exposure period of many years. The images in Figure 17 show a sunroom with a painting (composed of single colorants) exposed to light from above. The uneven irradiance across the surface of the painting was computed using a standard global illumination algorithm. Figure 1 depicts a newspaper exposed over an extended period of light exposure ($2.789 \times 10^7\,J\,m^{-2}$). The newsprint was folded in quarters during exposure, resulting in an uneven pattern of yellowing. The fading parameters used are given in Tables II and III.

Figure 18 shows a bulletin board. Printed materials have been added and removed from the bulletin board over time. While a printed material is in place, the area of the bulletin board covered by it is shielded from fading effects, resulting in a dark patch whose color depends on the period of light exposure. The fading parameters used are given in Tables II and III.

6.4 Limitations

The proposed framework is directed at simulating the changes in appearance of materials due to extended periods of light exposure. Although exposure to light is arguably one of the primary causes of fading of pigments, other factors such as heat or humidity may also influence fading. Our framework as proposed does not account for these effects.

To the best of our knowledge, detailed data regarding the light-fastness of particular colorants is unavailable. Lightfastness data typically consists of a rating on a subjective scale. The rating is

Fig. 18. A sequence of renderings of a bulletin board in which printed materials have been added and removed over time, leaving an irregular fading pattern on the cork. A comic strip clipped from a newsprint has also yellowed from the prolonged light exposure. Some textures used with permission of Turbosquid [2009].

obtained by fading the sample under consideration next to a test card consisting of blue wool samples of varying degrees of light-fastness [Choudhury 2006]. Moreover, such data is not typically published for commercially available materials. As a result, it was necessary to fit the parameters used in our model using regression techniques [Kenney and Keeping 1962]. In many fields, regression techniques are used to overcome data scarcity limitations [Lazár and Schansker 2009; Shi and DiMarzio 2007; Hallik et al. 2009]. We remark that although the values assigned for the parameters were selected to highlight appearance features, these parameters have a physical basis. This allows the scope of applications of the proposed framework to be extended to predictive rendering as described by Greenberg et al. [1997] in their seminal work on predictability.

7. CONCLUSION AND FUTURE WORK

The appearance of a material is determined by how it scatters and absorbs light. In traditional computer graphics, the appearance of a material is considered at a given instant in time. Over extended periods of time, however, light can alter the physicochemical properties of a material, leading to noticeable changes in its appearance. Among these changes, fading is one of the most ubiquitous in real-world settings. In this article, we have presented a novel theoretical framework for the underlying mechanisms responsible for the fading of surface finishes, such as paints and stains, due to light exposure. This framework describes the kinetics of fading processes using a robust, yet flexible physicochemical approach that allows for a wide range of variations in light exposure levels and sample conditions such as thickness and colorant (single or mixture) contents.

The proposed framework provides the foundation for predictive simulations of time-dependent light exposure effects on material appearance, aimed not only to computer graphics applications, but also to conservation and industrial investigations. In this work, these simulations are realized through the development of a layered fading model using the K-M formulation [Kubelka and Munk 1931]. To evaluate the fidelity of this model, its readings were compared to spectrophotometric measurements obtained from a fading experiment performed during this research. The qualitative agreement between the simulated and measured results indicates that the theoretical treatment given to fading in this article can capture a variety of different fading behaviors.

On the application side, the layered fading model introduced in this work can be readily integrated into existing image synthesis pipelines. In addition, its deterministic nature makes it suitable for inversion procedures aimed at the derivation of colorant time-varying parameters. To solve the system of differential equations describing the effects of light exposure on material appearance over time, we have proposed an efficient numerical strategy that takes advantage of the layered structure of the proposed framework. To demonstrate the applicability of this model, we have rendered several typical scenes depicting man-made objects subjected to light exposure during extended periods of time.

It should be noted that the proposed framework is limited to accounting for changes at the site in which light absorption takes place. For instance, the removal of a colorant at the site of absorption may cause adjacent colorant to spread in order to reach an equilibrium. Additionally, in organic materials, the absorption of light may induce reactions that affect the medium at locations other than the site of absorption. In future work, we plan to extend the proposed framework to address these limitations. We also intend to explore its application for simulating changes to other material appearance attributes, such as fluorescence, induced by absorbed radiation. Additionally, we plan to investigate the techniques for inverting the simulation procedures described in this article. This would enable its application in studies aimed at digital restoration of faded artifacts. We are confident that the proposed framework sets a firm foundation for these extensions to be built upon.

APPENDIX

A. COMPUTING THE KUBELKA-MUNK PARAMETERS FROM REFLECTANCE MEASUREMENTS

To compute the K-M absorption and scattering coefficients, we use a procedure based on techniques described by Johnston-Feller [2001]. First, we measure the reflectance of a layer of known thickness over a black substrate with reflectance ρ_b and over a white reflectance standard, such as spectralon (which we assume to have unit reflectance). Let ρ_0 and ρ_1 denote these reflectance measurements, respectively. According to K-M theory, the reflectance of a layer of finite thickness is given by

$$\rho = \frac{1 - \rho_g(a - b \coth b\mu^s Z)}{a + b \coth b\mu^s Z - \rho_g}, \tag{37}$$

where ρ_g is the reflectance of the substrate, Z is the thickness of the layer, and

$$a = \frac{\mu^a + \mu^s}{\mu^a}, \qquad (38)$$

$$b = \sqrt{a^2 - 1}. \qquad (39)$$

To simplify Eq. (37), we define

$$x_1 = a - b \coth b\mu^s Z, \qquad (40)$$

$$x_2 = a + b \coth b\mu^s Z. \qquad (41)$$

Note that

$$a = \frac{x_1 + x_2}{2}. \qquad (42)$$

This reduces Eq. (37) to

$$\rho = \frac{1 - x_1 \rho_g}{x_2 - \rho_g}. \qquad (43)$$

From our reflectance measurements, we have

$$\rho_0 = \frac{1 - x_1 \rho_b}{x_2 - \rho_b}, \qquad (44)$$

$$\rho_1 = \frac{1 - x_1}{x_2 - 1}. \qquad (45)$$

The unknowns x_1 and x_2 may be determined by solving

$$\begin{pmatrix} \rho_b & \rho_0 \\ 1 & \rho_1 \end{pmatrix} \begin{pmatrix} x_1 \\ x_2 \end{pmatrix} = \begin{pmatrix} 1 + \rho_0 \rho_b \\ 1 + \rho_1 \end{pmatrix}. \qquad (46)$$

Now a and b may be computed using Eqs. (42) and (39), respectively. The scattering and absorption coefficients may then be derived from Eqs. (41) and (38), respectively, and are given by

$$\mu^s = \frac{1}{bZ} \coth^{-1} \frac{x_2 - a}{b}, \qquad (47)$$

$$\mu^a = (a - 1)\mu^s. \qquad (48)$$

ACKNOWLEDGMENTS

REFERENCES

ABDUL-RAHMAN, A. AND CHEN, M. 2005. Spectral volume rendering based on the Kubelka-Munk theory. *Comput. Graph. Froum 24*, 3, 413–422.

BOSCH, C., LAFFONT, P., RUSHMEIER, H., DORSEY, J., AND DRETTAKIS, G. 2011. Image-Guided weathering: A new approach applied to flow phenomena. *ACM Trans. Graph. 30*, 3, 20:1–13.

CHEN, Y., XIA, L., WONG, T., TONG, X., BAO, H., GUO, B., AND SHUM, H. 2005. Visual simulation of weathering by γ-ton tracing. *ACM Trans. Graph. 24*, 3, 1127–1133.

CHOUDHURY, A. 2006. *Textile Preparation and Dyeing*. Science Publishers, Enfield, NH.

CURTIS, C., ANDERSON, S., SEIMS, J., FLEISCHER, K., AND SALESIN, D. 1997. Computer-Generated watercolor. In *Computer Graphics Proceedings*. Annual Conference Series, 421–430.

DOI, M. AND TOMINAGA, S. 2003. Spectral estimation of human skin color using the Kubelka-Munk theory. In *Proceedings of SPIE*. Vol. 5008, 221–228.

DORSEY, J. AND HANRAHAN, P. 1996. Modeling and rendering of metallic patinas. In *Computer Graphics Proceedings*. Annual Conference Serie, 387–396.

DORSEY, J., PEDERSEN, H., AND HANRAHAN, P. 1996. Flow and changes in appearance. In *Computer Graphics Proceedings*, Annual Conference Series, 411–420.

DORSEY, J., RUSHMEIER, H., AND SILLION, F. 2008. *Digital Modeling of Material Appearance*. Morgan Kaufmann/Elsevier.

GILES, C. 1965. The fading of colouring matters. *J. Appl. Chemi. 15*, 541–550.

GILES, C., JOHARI, D., AND SHAH, C. 1968. Some observations on the kinetics of dye fading. *Textile Res. J. 38*, 10, 1048–1056.

GILES, C. AND MCKAY, R. 1963. The lightfastness of dyes: A review. *Textile Res. J. 33*, 7, 528–575.

GLADING, R. 1940. The ultraviolet absorption spectra of lignin and related compounds. Ph.D. thesis, The Institute of Paper Chemistry, Lawrence College, Appleton, WI.

GREENBERG, D., ARVO, J., LAFORTUNE, E., TORRANCE, K., FERWERDA, J., WALTER, B., TRUMBORE, B., SHIRLEY, P., PATTANAIK, S., AND FOO, S. 1997. A framework for realistic image synthesis. In *Computer Graphics Proceedings*. Annual Conference Series, 477–494.

GROSSWEINER, L., GROSSWEINER, J., AND ROGERS, B. 2005. *The Science of Phototherapy: An Introduction*. Springer.

GU, J., TU, C.-I., RAMAMOORTHI, R., BELHUMEUR, P., MATUSIK, W., AND NAYAR, S. 2006. Time-Varying surface appearance: Acquisition, modeling and rendering. *ACM Trans. Graph. 25*, 3, 762–771.

HAASE, C. AND MEYER, G. 1992. Modeling pigmented materials for realistic image synthesis. *ACM Trans. Graph. 11*, 4, 305–335.

HALLIK, L., KULL, O., NILSON, T., AND NUELAS, J. P. 2009. Spectral reflectance of multispecies herbaceous and moss canopies in the boreal forest understory and open field. *Canad. J. Remote Sens. 35*, 5, 474–485.

HANRAHAN, P. AND KRUEGER, W. 1993. Reflection from layered surfaces due to subsurface scattering. *Comput. Graph. 27*, 165–174.

HAŠAN, M., FUCHS, M., MATUSIK, W., PFISTER, H., AND RUSINKIEWICZ, S. 2010. Physical reproduction of materials with specified subsurface scattering. *ACM Trans. Graph. 29*, 4, 61:1–10.

HEITNER, C. 1993. Light-Induced yellowing of wood-containing papers. In *Photochemistry and Lignocellulosic Materials*, C. Heitner and J. Scaiano, Eds., ACS Symposium Series, vol. 531, American Chemical Society, Washington, DC, 2–25.

HUNGER, K. AND WILKER, G. 2004. *Industrial Organic Pigments: Production, Properties and Applications*, 3rd Ed. Wiley-VCH, Weinheim, Germany.

IMAI, F., ROSEN, M., AND BERNS, R. 2001. Multi-Spectral imaging of a Van Gogh's self-portrait at the National Gallery of Art, Washington, D.C. In *Proceedings of the IS&T PICS Conference*. IS&T, 185–189.

ISAACSON, E. AND KELLER, H. 1994. *Analysis of Numerical Methods*. Dover Publications.

JOHNSTON-FELLER, R. 1986. Reflections on the phenomenon of fading. *J. Coat. Technol. 58*, 736, 33–50.

JOHNSTON-FELLER, R. 2001. *Color Science in the Examination of Museum Objects: Nondesctructive Procedures*. Tools for Conservation Series. The Getty Conservation Institute, Los Angeles, CA.

JOHNSTON-FELLER, R., FELLER, R., BAILIE, C., AND CURRAN, M. 1984. The kinetics of fading: Opaque paint films pigmented with alizarin lake and titanium dioxide. *J. Amer. Inst. Conserv. 23*, 2, 114–129.

KENNEY, J. AND KEEPING, E. 1962. *Mathematics of Statistics* 3rd Ed. Van Nostrand, Princeton, NJ.

KIDER, J., RAJA, S., AND BADLER, N. 2011. Fruit senescence and decay simulation. *Comput. Graph. Forum 30,* 2, 257–266.

KUBELKA, P. 1948. New contributions to the optics of intensly light-scattering materials. Part I. *J. Opti. Soc. Amer. 38,* 5, 448–457.

KUBELKA, P. AND MUNK, F. 1931. Ein beitrag zur optik der farbanstriche (An article on optics of paint layers). *Zeitschrift für Technische Physik 12,* 593–601.

LAZÁR, D. AND SCHANSKER, G. 2009. Models of chlorophyll a fluorescence transients. *Advances in Photosynthesis and Respiration,* vol. 29, Springer Science+Business Media B.V., 85–123.

LEARNER, T., SMITHEN, P., KRUEGER, J., AND SCHILLING, M., Eds. 2008. *Modern Paints Uncovered.* Getty Publications, Los Angeles, CA.

MÉRILLOU, S. AND GHAZANFARPOUR, D. 2008. A survey of aging and weathering phenomena in computer graphics. *Comput. Graph. 32,* 2, 159–174.

MORRIS, H. AND WHITMORE, P. 2007. "Virtual fading" of art objects: Simulating the future fading of artifacts by visualizing micro-fading test results. *J. Ameri. Insti. Conserv. 46,* 215–228.

MORTON, T. 1949. The practical assessment of the light fastness of dyeings. *J. Soci. Dyers Colouri. 62,* 12, 597–605.

PEREIRA, H. 2007. *Cork: Biology, Production and Uses.* Elsevier, Oxford, UK.

POLYANIN, A. AND ZAITSEV, V. 2004. *Handbook of Nonlinear Partial Differential Equations.* Chapman & Hall/CRC, Boca Raton, FL.

ROBERTS, J. 1996. *The Chemistry of Paper.* The Royal Society of Chemistry, Cambridge, UK.

RÅNBY, B. AND RABEK, J. 1975. *Photodegredation, Photo-Oxidation, and Photostabilization of Polymers.* John Wiley & Sons.

RUDOLF, D., MOULD, D., AND NEUFELD, E. 2003. Simulating wax crayons. In *Proceedings of the Pacific Conference on Computer Graphics and Applications.* 163–172.

SAUNDERSON, J. 1942. Calculation of the color of pigmented plastics. *J. Opti. Soci. Ameri. 32,* 12, 727–729.

SEYFRIED, M. AND FUKSHANSKY, L. 1983. Light gradients in plant tissue. *Appli. Optics 22,* 9, 1402–1408.

SHI, T. AND DIMARZIO, C. 2007. Multispectral method for skin imaging: development and validation. *Appli. Optics 46,* 36, 8619–8626.

SHI, X. AND LU, D. 2005. Colorimetric and chemical modeling based aging simulation of Dunhuang murals. In *Proceedings of the 5th International Conference on Computer and Information Technology.* 570–574.

SHI, X., LU, D., AND LIU, J. 2006. Color changing and fading simulation for frescoes based on empirical knowledge from artists. In *Advances in Multimedia Information Processing - PCM 2006.* Lecture Notes in Computer Science, vol. 4261. Springer. 861–869.

THOMSON, G. 2002. *The Museum Environment,* 2nd ed. Butterworth-Heinemann, Oxford, U.K.

TURBOSQUID (USER: AZDESIGNSTUDIO). 2006. Pavers. http://www.turbosquid.com/FullPreview/Index.cfm/ID/318374.

TURBOSQUID (USER: FWORX). 2004. Blinds. http://www.turbosquid.com/3d-models/free-blinds-3d-model/243419.

TURBOSQUID (USER: POLYGONISTA). 2010 Newspaper. http://www.turbosquid.com/3d-models/maya-newspaper-news/567189.

TURBOSQUID (USER: RES_COM_3D). 2009. End table. http://www.turbosquid.com/3d-models/end-table-3ds-free/451642.

TURBOSQUID (USER: SCORCHEDMEDIA). 2007. Couch. http://www.turbosquid.com/3d-models/couch-chaise-3ds-free/368829.

TURBOSQUID (USER: TRIPRAY COMPANY). 2009. Cork a-017. http://www.turbosquid.com/FullPreview/Index.cfm/ID/463083.

WANG, J., TONG, X., LIN, S., PAN, M., WANG, C., BAO, H., GUO, B., AND SHUM, H.-Y. 2006. Appearance manifolds for modeling time-variant appearance of materials. *ACM Trans. Graph. 25,* 3, 754–761.

WHITMORE, P. AND BAILIE, C. 1997. Further studies on transparent glaze fading: Chemical and appearance kinetics. *J. Ameri. Insti. Conserv. 36,* 3, 207–230.

WHITMORE, P., PAN, X., AND BAILIE, C. 1999. Predicting the fading of objects: Identification of fugitive colorants through direct nondestructive lightfastness measurements. *J. Ameri. Insti. Conserv. 38,* 3, 395–409.

XUE, S., DORSEY, J., AND RUSHMEIER, H. 2011. Stone weathering in a photograph. In *Proceedings of the Eurographics Symposium on Rendering.* R. Ramamoorthi and E. Reinhard, Eds., 1189–1196.

YANG, L. 2003. Characterization of inks and ink application for ink-jet printing: Model and simulation. *J. Opti. Soci. Amer. 20,* 7, 1149–1154.